Organic & Biomolecular Chemistry

PAPER

View Article Online
View Journal | View Issue

Cite this: *Org. Biomol. Chem.*, 2015, **13**, 4605

Small gold nanoparticles for interfacial Staudinger–Bertozzi ligation†

Pierangelo Gobbo,*[a] Wilson Luo,[a] Sung Ju Cho,[a] Xiaoxiao Wang,[a] Mark C. Biesinger,[b] Robert H. E. Hudson[a] and Mark S. Workentin*[a]

Received 24th February 2015,
Accepted 11th March 2015

DOI: 10.1039/c5ob00372e

www.rsc.org/obc

Small gold nanoparticles (AuNPs) that possess interfacial methyl-2-(diphenylphosphino)benzoate moieties have been successfully synthesized (Staudinger-AuNPs) and characterized by multi-nuclear MR spectroscopy, transmission electron microscopy (TEM), UV-Vis spectroscopy, thermogravimetric analysis, and X-ray photoelectron spectroscopy (XPS). In particular, XPS was remarkably sensitive for characterization of the novel nanomaterial, and in furnishing proof of its interfacial reactivity. These Staudinger-AuNPs were found to be stable to the oxidation of the phosphine center. The reaction with benzyl azide in a Staudinger–Bertozzi ligation, as a model system, was investigated using ^{31}P NMR spectroscopy. This demonstrated that the interfacial reaction was clean and quantitative. To showcase the potential utility of these Staudinger-AuNPs in bioorganic chemistry, a AuNP bioconjugate was prepared by reacting the Staudinger-AuNPs with a novel azide-labeled CRGDK peptide. The CRGDK peptide could be covalently attached to the AuNP efficiently, chemoselectively, and with a high loading.

The conjugation of biomolecules to nanomaterials is of high interest because of the potential applications of the resulting bioconjugate in biological and medical diagnostics, therapeutics and drug vectors.[1–5] Among all nanomaterials, gold nanoparticles are often regarded as the most promising template because of their low toxicity and chemical stability. In addition, their optical properties can be easily tuned by varying the gold core diameter[6] and the chemical properties can be tuned by changing the ligand corona.[7] In the past decade, many different approaches have been developed to synthesize AuNP bioconjugates for different purposes. Generally these strategies rely on electrostatic interactions between the gold surface and the side chains of the biomolecule's residues, on hydrophobic–hydrophilic type of interactions, on direct place exchange exploiting the affinity of cysteine for gold, or on interfacial reactions (*e.g.* interfacial EDC coupling, imine formation *etc.*).[8] These methods generally result in an uncontrolled "shotgun" type bioconjugation,[9] whereas for many applications it is desirable to have more precise control over the amount of biomolecule that is introduced. This can be achieved by designing a single stable AuNP that exhibits a chemoselective reactive moiety at its interface that serves as an anchoring group to incorporate a discrete number of biomolecules. This could result in the precise tuning of the final biophysical properties of the AuNP-bioconjugate. It is also desirable that the interfacial reactive group on the nanoparticle leads to a robust conjugate that relies on a strong bond between nanoparticle and biomolecule. In order for the interfacial reaction to be chemoselective, this nanoparticle template must undergo a reaction with a functional group that is not present in nature, atoxic, and small so that it does not affect the activity of the conjugated biomolecule.

The functionality that addresses all these requirements is the azide group. The azide can undergo four different reactions. The [3 + 2] Huisgen cycloaddition and the copper catalyzed [3 + 2] Huisgen cycloaddition with dipolarophiles, the strained-promoted alkyne–azide cycloaddition (SPAAC) with strained alkynes and the Staudinger–Bertozzi ligation.[10,11] While the [3 + 2] Huisgen cycloaddition and its catalyzed version are not completely compatible with AuNPs chemistry because the high temperature or the Cu(I) required to push the reaction to completion cause severe nanoparticle aggregation,[12] the SPAAC reaction presents limited chemoselectivity due to the possibility of nucleophilic attacks (especially from thiols and amines largely present in biomolecules) to the highly reactive strained triple bond.[13–15] A recent work of ours

[a]*The University of Western Ontario and the Centre for Materials and Biomaterials Research, Richmond Street, London, Ontario, Canada. E-mail: mworkent@uwo.ca, pgobbo2@uwo.ca; Tel: +1 519-661-2111 extn 86319*
[b]*Surface Science Western, The University of Western Ontario, 999 Collip Circle, London (ON), N6G 0J3, Canada*

†Electronic supplementary information (ESI) available: Detailed synthesis and characterization of the methyl-2-(diphenylphosphino)benzoate-thiol ligand; detailed procedure for the synthesis of the Staudinger-AuNP; TGA data; complete XPS characterization for the Staudinger-AuNP, the Staudinger-AuNP reacted with benzyl azide, and Staudinger-AuNP reacted with peptide; details of the calculations for the nanoparticles raw formula; detailed synthesis and characterization of the azide-modified peptide. See DOI: 10.1039/c5ob00372e

highlighted this issue showing how post assembly deprotection of peptides once "clicked" on the AuNP surface was necessary to efficiently synthesize a nanoparticle bioconjugate through the SPAAC reaction.[16] The Bertozzi–Staudinger ligation is a reaction that was specifically developed for investigating the metabolic engineering of cell surfaces[17] and takes place between the azide and a substituted triphenylphosphine. Whereas the cycloaddition reactions lead to a triazole ring, the Staudinger–Bertozzi ligation forms a stable amide bond. From its very first development the Staudinger–Bertozzi ligation has been successfully employed in biochemistry to immobilize peptides and proteins onto different materials,[18–22] for *in vivo* and *in vitro* imaging, and for protein detection.[23–25]

This reaction seems to be an ideal candidate for designing a new AuNP template that can react in a highly chemoselective and efficient way with any azide-modified (bio)molecule. For these reasons we report the synthesis of a thiol ligand that contains a methyl-2-(diphenylphosphino)benzoate moiety designed to undergo a Staudinger–Bertozzi ligation with azide functionalities. This ligand was introduced onto the surface of small water-soluble AuNPs through a place-exchange reaction and the reactivity of the resulting nanomaterial was investigated using benzyl azide as model clickable partner. Finally, to showcase the high chemoselectivity of these novel reactive AuNPs for bioconjugation, we react them with an azide-modified CRGDK peptide. CRGDK peptides are promising targeting biomolecules for diverse cancer cells lines and therefore the resulting AuNP-CRGDK bioconjugate would be a potential broad-spectrum targeting agent.[1] In addition, the presence of the cysteine in the CRGDK peptide represents a challenge for the chemoselective conjugation on nanoparticles. Herein, we present a facile, versatile, and straightforward protocol for the conjugation of biomolecules onto the AuNP surface through the Staudinger–Bertozzi ligation. Importantly, the study showcases the use of XPS as a method to easily characterize the interfacial reactivity of this new nanomaterial, and to quantify the amount of conjugated biomaterial, information that is very important for practical applications in biochemistry, medical diagnosis, therapies and drug delivery.

Results and discussion

The approach used to introduce the reactive triphenylphosphine moiety for the Staudinger–Bertozzi ligation onto the water-soluble AuNPs required the synthesis of the appropriate thiol containing ligand for a place-exchange reaction; see Scheme 1. The first step involved coupling 3-(diphenylphosphino)-4-(methoxycarbonyl)benzoic acid (**1**) to an amino-tetraethylene glycol-trityl-protected thiol (**2**). The deprotection of the thiol functionality in 5% trifluoroacetic acid–dichloromethane led to the desired phosphine-thiol ligand (**4**). Details of the ligand synthesis can be found in the ESI.† Compound (**4**) was found to be remarkably stable to the oxidation of both phosphine and thiol ends. Attempts to oxidize the phosphine and the thiol by dissolving the molecule in wet solvents and by air bubbling failed. However, small amounts of phosphine oxide can form during the different stages of the ligand synthesis. It was possible to reduce the phosphine oxide back to the active phosphine using the synthetic procedure reported by H.-C. Wu *et al.*[26] Before deprotecting the thiol end, the mixture of phosphine oxide and phosphine can be dissolved in a solution of triphenylphosphine and $HSiCl_3$ in dry toluene. Heating of this reaction mixture to 100 °C leads to the quantitative reduction of the phosphine oxide. It is noteworthy that this reaction fails in presence of free thiols and, if the phosphine-oxide reduction is carried out at the nanoparticles interface, $HSiCl_3$ causes a fast and total decomposition of the AuNP.

The Staudinger-AuNPs have been synthesized through a place-exchange reaction using triethylene glycol monomethyl ether AuNP (MeO-EG_3-AuNP) as the starting material, Scheme 1. Details of their synthesis of the latter can be found in the ESI.† These nanoparticles have a gold core diameter of 3 ± 1 nm and are soluble in water and polar organic solvents.[27] MeO-EG_3-AuNPs represent a very resilient substrate for further modification and interfacial organic chemistry because they are resistant to acidic[16] and basic conditions,[12] they can be heated to over 100 °C,[27] and they can be repeatedly dried and re-dissolved in a solvent with little to no aggregation. The place-exchange reaction to introduce the phosphine-thiol (**4**) onto the nanoparticle's corona was carried out by dissolving 200 mg of MeO-EG_3-AuNP and 100 mg of phosphine-thiol (**4**) in dry and argon purged dichloromethane. The reaction was carried out for 15 minutes at room temperature, under inert atmosphere (to minimize potential oxidation of the reactive phosphine) and under vigorous stirring. The particles were then cleaned from the excess thiol by re-dissolving them in 6 ml of dichloromethane and by precipitating them by adding 33 ml of hexanes in which the nanoparticles are not soluble. This washing operation was repeated five times overall. The Staudinger-AuNPs were characterized by ^{1}H and ^{31}P NMR spectroscopy, transmission electron microscopy (TEM), UV-Vis spectroscopy, thermogravimetric analysis, and X-ray photoelectron spectroscopy (XPS). The ^{1}H and ^{31}P NMR spectra showed presence of broad peaks typical of a AuNP sample indicating that the washing procedure was efficient and that the most of the free thiol ligands were successfully removed. Curiously the spectra did not show a perfect correspondence of the peaks with the free ligand (**4**). Usually the successful incorporation of a second thiol ligand through the place-exchange reaction is easily determined by comparing the ^{1}H NMR spectra of the free ligand with that of the place-exchanged AuNPs sample. The chemical shifts typically match even though the peaks on the AuNPs spectrum are broader.[28,29] In this case ^{1}H NMR spectrum shows a substantial difference in the aromatic region as highlighted in Fig. 1. An even more drastic difference is observed in the ^{31}P NMR spectrum of the Staudinger-AuNPs with respect to that of compound (**4**). The ^{31}P NMR spectrum of the Staudinger-AuNPs did not show a peak for the phosphine at −3.8 ppm, but two signals one broad and intense at 40.3 ppm and one at 31.3 ppm. By

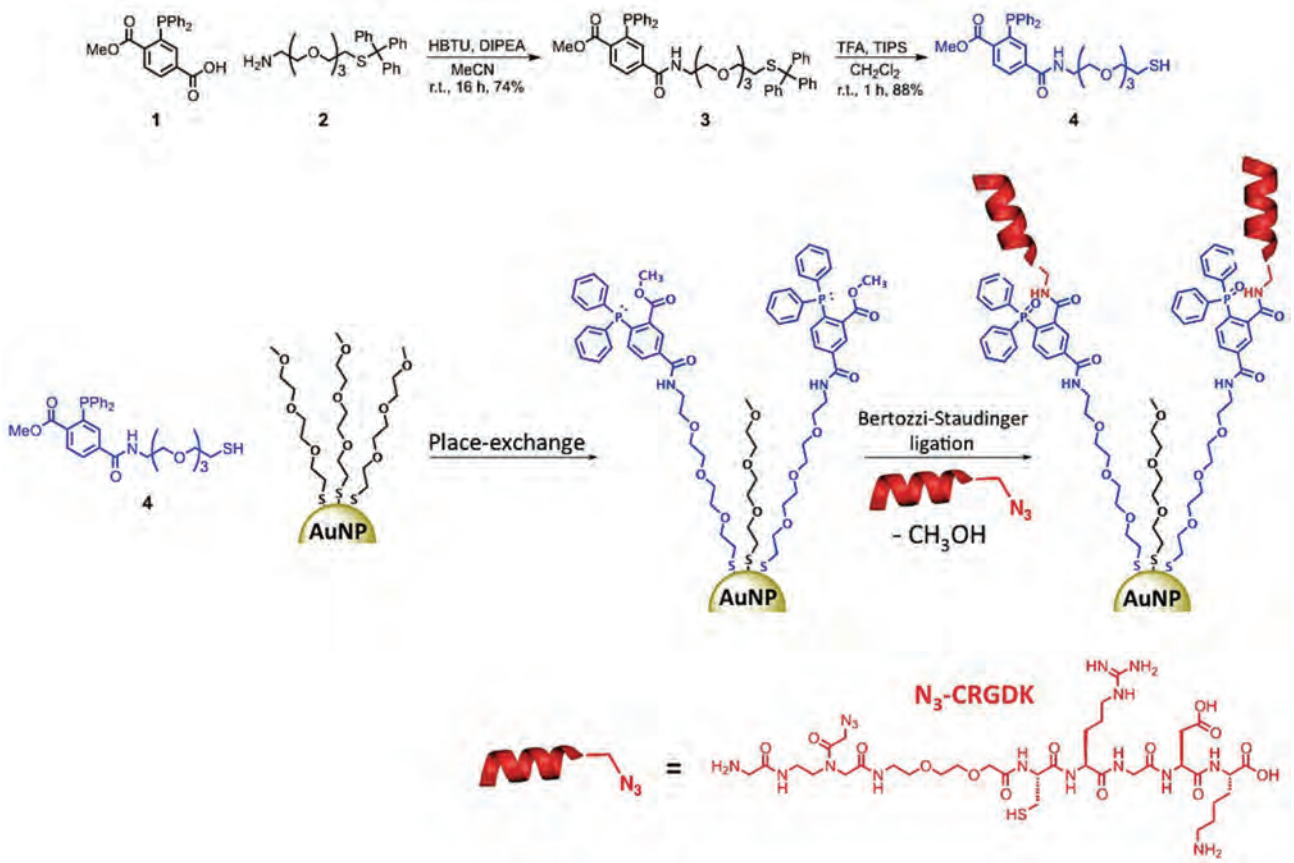

Scheme 1 Synthetic strategy for the synthesis of the Staudinger-AuNP.

comparison with the data of the phosphine oxide formation gathered during the synthesis of compound (**4**), the signal at 31.3 ppm can be attributed to the oxidized methyl-2-(diphenylphosphino)benzoate. Integration of the ^{31}P NMR peaks shows that the AuNP sample has 9% of oxidized phosphine that is most likely generated during the washing procedure where it is exposed to air. The shift of the phosphine peak in the ^{31}P NMR and the difference in the aromatic region shown in the ^{1}H NMR seem to suggest that there is an interaction at the phosphorous center that changes the electronic properties of the phosphine.

Transmission electron microscopy provided relevant insights on this issue. The TEM images reported in Fig. 3A clearly show that 3.63 ± 1.4 nm Staudinger-AuNPs are interacting with each other forming AuNPs self-assemblies with an inter-particle distance of ~1 nm.[30,31] TEM images of similar ethylene glycol small AuNPs usually show well isolated and evenly distributed dark spots on the TEM grid, like after the interfacial Staudinger–Bertozzi ligation, see Fig. 3B. This AuNPs self-assembly was also confirmed by UV-Vis spectroscopy. Typically AuNPs of such a small size do not show any plasmon resonance band in the UV-Vis spectrum. However, the UV-Vis derivative reported in Fig. 3C highlights the appearance of a weak plasmon band in the region 525–650 nm for the Staudinger-AuNP sample compared to the MeO-EG$_3$-AuNP starting material due to the very short distance between the gold cores involved in the AuNPs self-assemblies. The reason for this collective behavior of the Staudinger-AuNPs is probably due to hydrophobic–hydrophilic-type of interactions between the hydrophilic ethylene glycol linker and the strongly hydrophobic character of the triphenylphosphine. As reported by K. J. M. Bishop and coworkers, ligands with different solubility properties introduced through a place-exchange reactions do not distribute homogenously on the particle's corona but rather tend to form patches or groups. These patches are responsible for the formation of inter-nanoparticles hydrophobic "bonds" resulting in the self-assembly of nanoparticle islands (like in the present work) or chain-like structures.[31]

High-resolution XPS analysis, see Fig. SI3,† further confirms the presence of inter-nanoparticle interactions showing a peak for the Au 4f core line that displays two different components: a small component at 84.62 eV typical of isolated AuNPs and a larger component at 83.75 eV that is characteristic of bulk gold and is most likely related to the AuNP networks shown in the TEM images.[32] XPS analysis also shows a peak for the amide nitrogen at 399.75 eV. The high resolution scans of the P 2p peak, see Fig. 4, shows a major component at 131.52 eV (P 2p$_{3/2}$) related to the triphenylphosphine and a minor component (13%) at 132.60 eV (P 2p$_{3/2}$) related to triphenylphosphine oxide, confirming independently and with

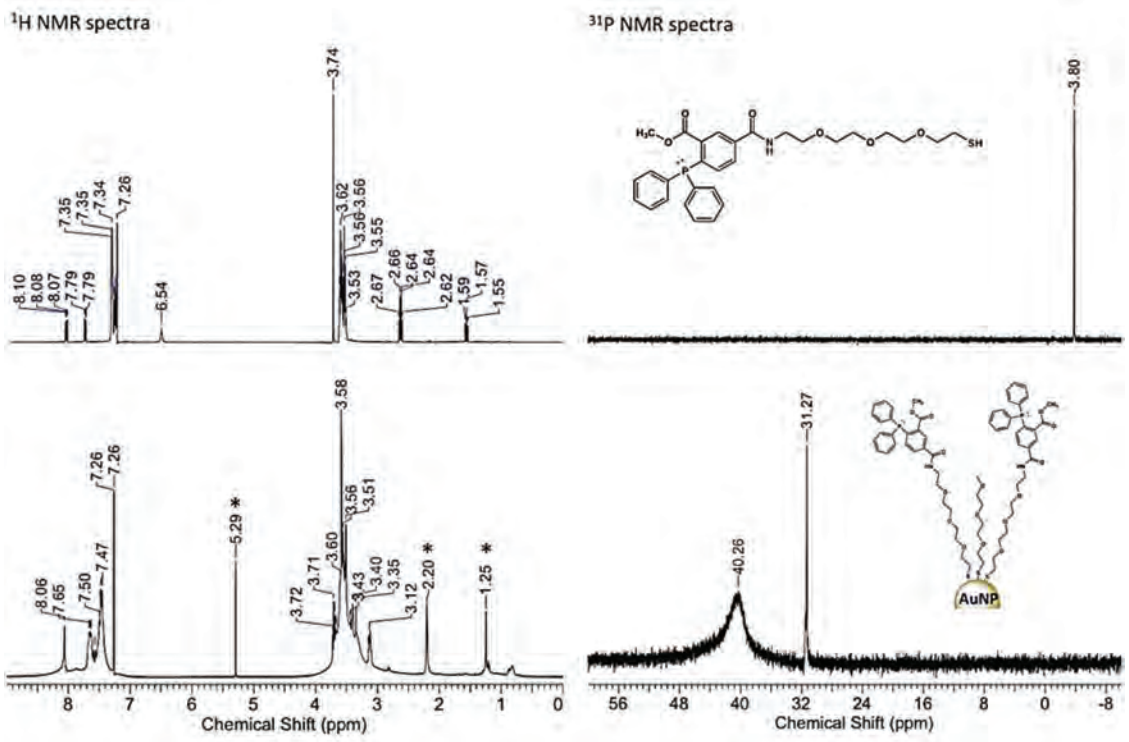

Fig. 1 ^{1}H (left) and ^{31}P (right) NMR spectra of phosphine-thiol (**4**) (top) *versus* Staudinger-AuNP (bottom). *Denotes residual solvent peaks. Spectra calibrated against residual chloroform and H_3PO_4.

higher precision the result obtained through ^{31}P NMR spectroscopy. The high resolution scans of the C 1s, see Fig. 4, shows a distinct component at 289.08 eV that is related to the carbonyl of the ester functional group, a component at 288.00 eV that is related to the amide's carbonyl, and the typical components for the ethylene glycol ligands at 286.36 eV and 285.00 eV. Finally, the high-resolution scan of the S 2p peak, see Fig. SI3,† shows the typical components of the sulfur–gold bond and presence of a negligible amount of free thiol and sulfates.[33] The presence of free thiols and sulfates (generated by the slow oxidation of thiols over time) is due to the fact that they have been trapped in between the AuNPs self-assemblies and are difficult to wash away.

Despite the peculiar behavior of these AuNPs, exposure to benzyl azide provided clear evidence of the Staudinger–Bertozzi product. In fact the peaks of the ^{1}H and ^{31}P NMR spectra returned to match those of the model Staudinger–Bertozzi product obtained using the phosphine-thiol (**4**) with benzyl-azide (*vide infra*).

Thermogravimetric analysis of the Staudinger-AuNP showed that the 43% of the total weight is due to the organic corona (see Fig. SI5†), of this the 60% is constituted by ligand (**4**), while the 40% is constituted by MeO-EG_3-S^-. Finally, from the deconvolution of the TGA curve, the ^{31}P NMR spectrum and the gold core diameter obtained from TEM images it was possible to calculate a raw formula for the Staudinger-AuNP: Au_{1500} (MeO-EG_3-S)$_{500}$ (Ph_3P-EG_4-S)$_{200}$ (Ph_3P═O-EG_4-S)$_{20}$. More specifically these Staudinger-AuNPs contain methyl-2-(diphenylphosphino)benzoate in concentration 0.432 μmol mg^{-1}. Details of these calculations are reported in the ESI.†

The reactivity of the Staudinger-AuNP through the Staudinger–Bertozzi ligation was then investigated using benzyl azide and the reactions were monitored through ^{31}P NMR spectroscopy. In the ^{31}P NMR spectrum it was possible to follow the disappearance of the broad peak at 40.3 ppm corresponding to the active phosphine and the appearance of the peak of the ligation product at 34.9 ppm, refer to Fig. 1 and 2. Kinetic experiments were carried out under pseudo-first-order reaction conditions at 25 °C and the reaction kinetics at the AuNP interface was compared with that in solution using ligand (**4**) as a model compound. For this investigation Staudinger-AuNP (0.0259 M in phosphine, 30.0 mg of Staudinger AuNP) were reacted with benzyl azide (0.518 M) in wet $CDCl_3$. Chloroform was chosen due to the high solubility of the nanoparticles in this solvent that permitted the high AuNPs concentration required for the experiments. A reaction using the same conditions was carried out between model compound (**4**) and benzyl azide. This same reaction was then carried out at higher concentration using $CDCl_3$ and DMSO-d_6 as the solvents to compare the results with those previously reported in the literature.[34] Table 1 summarizes the results of these kinetic experiments. During the course of all these reactions no intermediates were observed through ^{31}P NMR spectroscopy. This indicates that the reaction mechanism remains

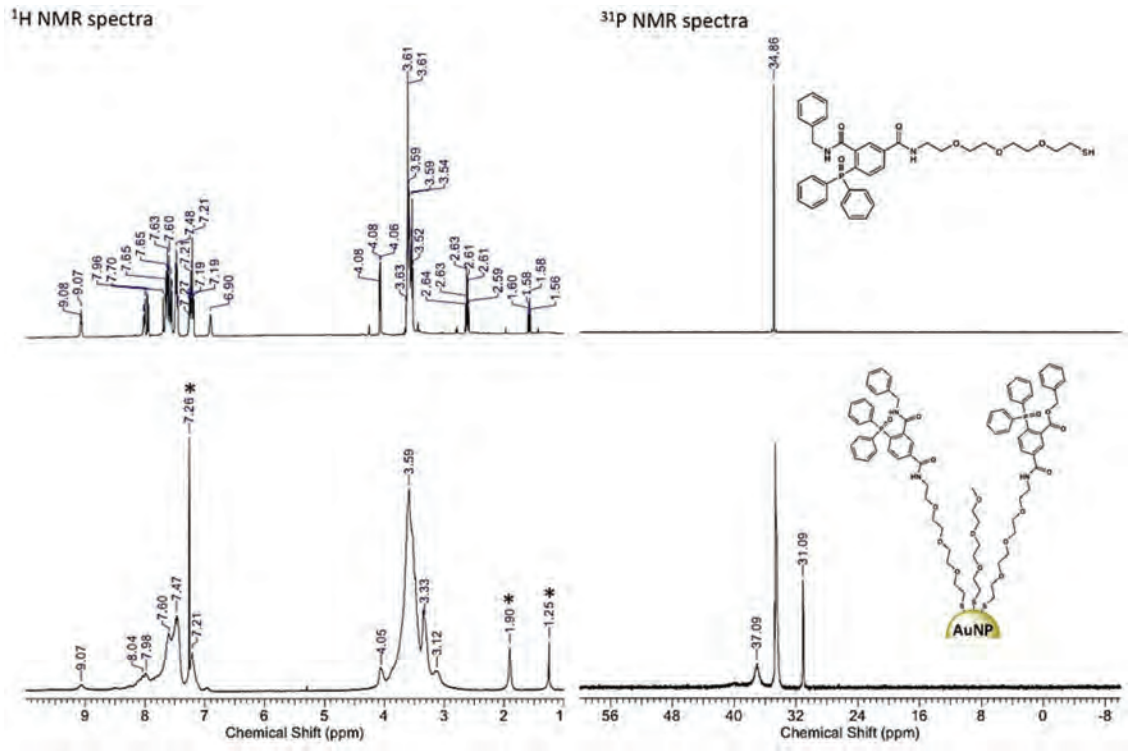

Fig. 2 ^{1}H (left) and ^{31}P (right) NMR spectra of phosphine-thiol (**4**) after reaction with benzyl azide (top) *versus* Staudinger-AuNP after reaction with benzyl azide (bottom). * Denotes residual solvent peaks. Spectra calibrated against residual chloroform and H_3PO_4.

Table 1 Second order rate constants of the Staudinger–Bertozzi ligation with benzyl azide obtained at 25 °C under different experimental conditions

	[Phosphine] (M)	[Benzyl azide] (M)	[H_2O] (M)	Solvent	Second order rate constant (10^{-3} M^{-1} s^{-1})
Staudinger-AuNP	0.0259	0.518	5.56	$CDCl_3$	0.027 ± 0.002
Ligand (**4**)	0.0259	0.518	5.56	$CDCl_3$	1.6 ± 0.1
Ligand (**4**)	0.0259	0.518	5.56	DMSO-d_6	3.5 ± 0.1
Ligand (**4**)	0.0440	0.830	5.56	DMSO-d_6	4.7 ± 0.1

that proposed by F. L. Lin and coworkers with the rate-limiting step being the formation of the phosphazide.[34] While this is not surprising for the model reactions with ligand (**4**), it is remarkable that the Staudinger–Bertozzi ligation takes place at the AuNPs interface in a comparable manner despite the markedly different chemical environment represented by the nanoparticle structure and the networks that they form in solution. Our results show that the reaction of ligand (**4**) has second-order rate constants comparable to those reported by F. L. Lin and coworkers and that they increase with an increase in solvent dielectric constant. The reaction at the AuNP interface instead results to be a hundred times slower. This is probably due to additional reaction parameters introduced with an interfacial reaction and because of the inter-nanoparticle interactions observed that need to be overcome before the ligation occurs. However, the interfacial phosphines are still reactive towards the Staudinger–Bertozzi ligation and the reaction yields the Staudinger–Bertozzi product quantitatively.

The product of the interfacial Staudinger–Bertozzi ligation was then separated from the free benzyl azide by washing a film of nanoparticles made in a round-bottom flask and rinsing it with hexanes where the nanoparticles are insoluble. The purified sample was then characterized by ^{1}H and ^{31}P NMR spectroscopy, XPS, UV-Vis spectroscopy and TEM. As anticipated, TEM images show the absence of AuNPs self-assemblies and only well isolated nanoparticles, see Fig. 3B. The ^{1}H NMR spectrum of the reacted Staudinger-AuNPs sample now shows perfect correspondence with the chemical shift of the model reaction with compound (**4**), see Fig. 2. The UV-Vis spectrum of the reacted nanoparticles sample now shows a spectrum similar to that of MeO-EG_3-AuNP starting material, characterized by the absence of a plasmon resonance band in the region 525–650 nm (see Fig. 3C).

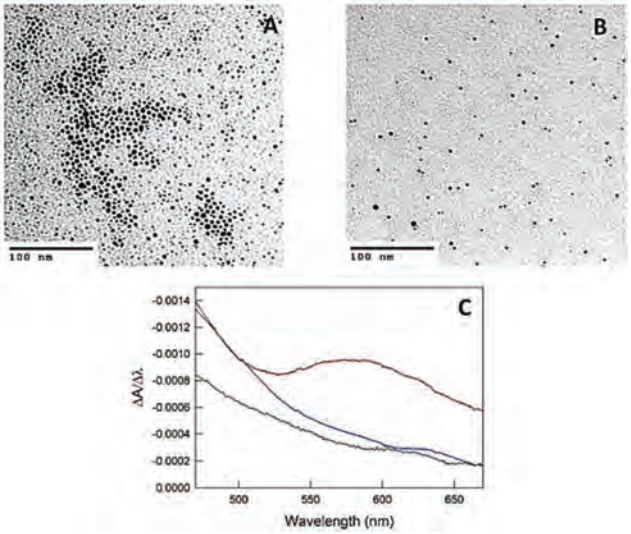

Fig. 3 TEM images of (A) Staudinger-AuNP, and (B) Staudinger-AuNP after reaction with benzyl azide. (C) Derivative of UV-Vis spectrum of MeO-EG_3-AuNP (blue), Staudinger-AuNP (red), and Staudinger-AuNP after reaction with benzyl azide. The derivative highlights the presence of the plasmon resonance band for the Staudinger-AuNP sample due to the AuNPs self-assemblies.

XPS proves to be a powerful technique to furnish proof of interfacial reactivity. Fig. 4 shows that after the interfacial reaction with the azide, the C 1s core line no longer shows the component for the ester bond at 289.08 eV, and the component at higher binding energy is now that related to the newly formed amide at 288.00 eV. This is expected because of the generation of methanol that occurs during the reaction mechanism. In addition, the high-resolution scan of the P 2p core line now appears narrower and shows only the component for the triphenylphosphine-oxide. These results together confirm that the interfacial reaction went to completion. The high-resolution scan of the S 2p core line now shows the absence of free thiols and disulfides as a result of efficient trituration once the nanoparticles self-assemblies has been abrogated.

In summary, despite the peculiar inter-Staudinger-AuNPs interaction that leads to AuNPs self-assemblies and changes the electronic properties of the phosphine, the Staudinger-AuNP are still readily reactive towards the azide bioorthogonal partner as highlighted by the kinetic study using ^{31}P NMR spectroscopy and by the XPS analysis of the interfacial ligation product. More importantly, the reaction is quantitative as independently confirmed by ^{31}P NMR spectroscopy and XPS analysis, and the reacted Staudinger-AuNP could be recovered easily and quantitatively.

To showcase the high chemoselectivity of these Staudinger-AuNPs and their potential for bioconjugation, we reacted them with an azide functionalized CRGDK peptide. The CRGDK peptide was synthesized *via* standard Fmoc SPPS method and the azide functionality was coupled to the N-terminus. The AuNP bioconjugate was synthesized simply by mixing 20 mg of Staudinger AuNP (8.64 μmol of phosphine) with 30 μmol of azide-CRGDK in DMSO-d_6 at 37 °C. The reaction was monitored through ^{31}P NMR spectroscopy following the progressive

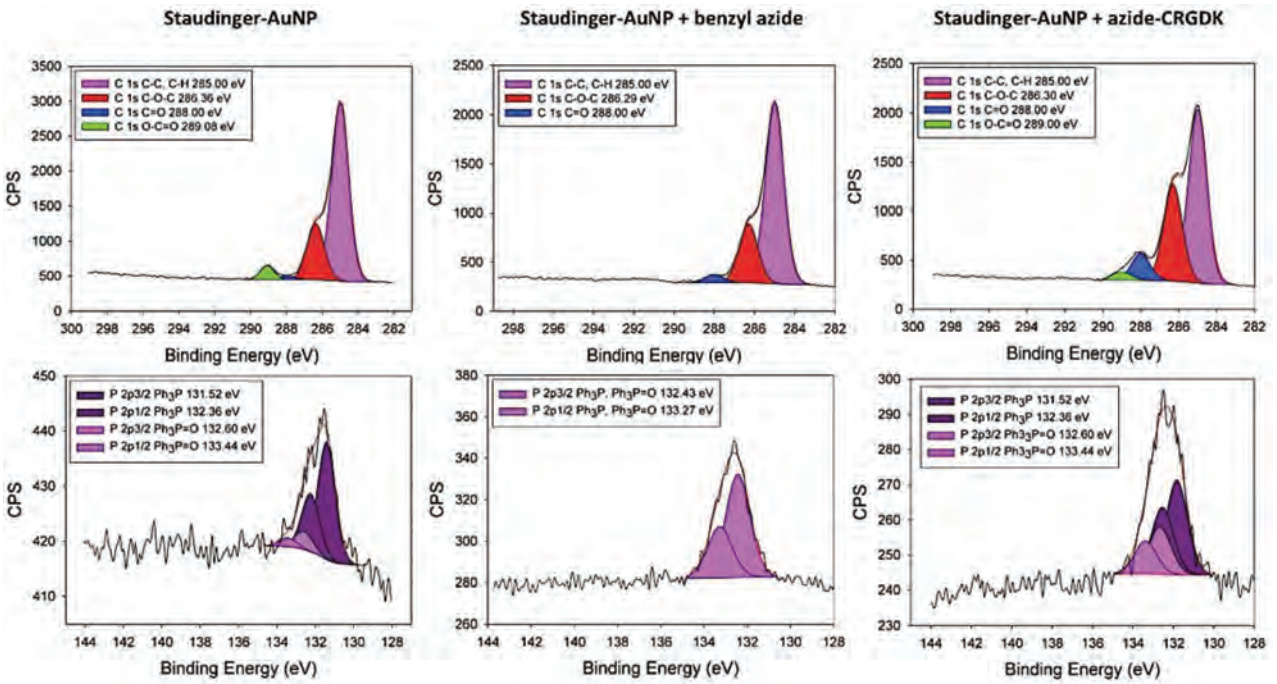

Fig. 4 High-resolution XPS of C 1s and P 2p core lines of the Staudinger-AuNP (left) and Staudinger-AuNP after reaction with benzyl azide (middle) and azide-CRGDK peptide (right).

disappearance of the broad peak at 40.3 ppm and the appearance of the product peak at 33.2 ppm (see Fig. SI11†) indicating proper interfacial reactivity with formation of the Staudinger–Bertozzi product. During the course of the reactivity we did not observe displacement of any of the AuNP ligands due to a place exchange reaction by the peptide's cysteine. This would have resulted in the appearance of a peak at −3.80 ppm for the free phosphine ligand and easily identifiable disulphides peaks in the ^{1}H NMR spectrum. When reaction was completed the excess peptide was washed away with nanopure water using centrifugal filtration (Millipore centrifugal filter units MWCO 10 kDa). Interestingly the reaction stopped at ~30% (calculated from the ^{31}P NMR spectra), indicating that most likely the AuNPs reached saturation due to the larger size of the peptide compared to the smaller model molecule benzyl azide. The AuNP-bioconjugate was characterized by TEM and XPS. TEM images (see Fig. SI10†) show again isolated AuNPs of ~3 nm in diameter and no nanoparticles networks were observed. The high-resolution scans of the C 1s peak (see Fig. 3) show still the presence of the ester component at 289.00 eV and a marked increase in the component related to amide's carbonyl at 288 eV due to the presence of the numerous peptide bonds. The high-resolution scans of the S 2p peak (see Fig. SI12†) now show a marked increase of the S–H component at 163.21 eV (S $2p_{3/2}$) and of the disulfide component at 168.45 eV (S $2p_{3/2}$)[33] due to the presence of the peptide's cysteines that do not interfere with the interfacial reactivity thanks to the high chemoselectivity of the Staudinger–Bertozzi ligation. Finally, the high-resolution scans of the P 2p peak confirms that the 30% of the phosphine reacted with the peptide to form the triphenylphosphine-oxide. Interestingly this 30% of interfacial reaction yield seems to be recurring when employing 3 nm AuNPs. The same result was indeed obtained when a DBCO-functionalized protected-peptide was clicked onto azide-functionalized AuNPs of the same size using the SPAAC-PAD strategy.[16] Because the smaller reactive partner (benzyl azide) reacted quantitatively, the lower extent of reaction with the peptide may simply be an issue of sterics with the peptide blocking additional reactive sites. These results together are consistent with successful conjugation of the peptide onto the Staudinger-AuNPs and the efficiency of the rinsing/trituration. Finally, the nanoparticle bioconjugate was found to be soluble in water and in polar organic solvents and could be repeatedly dried and redissolved in solvent with little to no aggregation.

Conclusions

In this paper we reported the first synthesis of small gold nanoparticles that present interfacial methyl-2-(diphenylphosphino)benzoate functionalities able to undergo Staudinger–Bertozzi ligation for the creation of nanoparticle bioconjugates. These small Staudinger-AuNPs were completely characterized and a nanoparticle raw formula could be estimated with good precision from the combination of the TGA data, NMR spectra and TEM images. This represents important information in the bioconjugation field because of the expense of both starting materials and consequent difficulty to work in excess of one or the other clickable partner.

The reactivity of the Staudinger-AuNP was then investigated through ^{31}P NMR spectroscopy using benzyl azide as the clickable partner. The possibility to easily monitor the reaction by ^{31}P NMR spectroscopy by following the disappearance of the phosphine peak at 40.3 ppm and the appearance of the phosphine oxide peak of the product at 34.9 ppm represents a great advantage of this novel nanomaterial, and makes their use easy and straightforward. The data obtained from the kinetic study showed that the reaction mechanism with which these AuNPs react appears to be identical to that of small methyl-2-(diphenylphosphino)benzoate molecules in solution. The only difference appears to be in the kinetic constant that resulted to be a hundred times slower, due to the interfacial character of the reaction. More importantly, these studies showed quantitative reactivity of the triphenylphosphine moieties with the azide partner small molecule and the reacted Staudinger-AuNPs could be quantitatively recovered.

XPS confirms to be a reliable and highly sensitive surface analysis technique for the study of interfacial organic chemistry. In fact, the Staudinger-AuNP and the successful formation of the interfacial ligation product could be effectively characterized through the high-resolution scans especially of the C 1s and the P 2p core lines. The former core line after the interfacial Staudinger–Bertozzi ligation clearly shows the disappearance of the component at 289.08 eV that corresponds to the methyl-ester functionality of the starting material; the latter distinctively show two components one for the triphenylphosphine at 131.52 eV and the other for the triphenylphosphine oxide at 132.43 eV, allowing for quantifying the amount of azide partner that has been clicked onto the nanoparticles.

Another great advantage of our Staudinger-AuNPs is the insensitivity of the Staudinger–Bertozzi ligation to nucleophiles such as thiols or amines that are largely present in biosystems. The high chemoselectivity of the Staudinger-AuNPs makes them an attractive alternative to faster but less chemoselective bioconjugation techniques that for example involve the Michael addition to maleimide functionalities or the SPAAC reaction. In fact, the reactivity of the maleimide or the side-reactivity of cyclooctyne towards thiols and amines can lower the chemoselectivity of the corresponding nanomaterial representing a threat to the biomolecule's conformation and biochemistry. In contrast our Staudinger-AuNPs react exclusively with the azide, as highlighted by the successful conjugation of an azide-functionalized CRGDK peptide. This direct conjugation would have required additional precautions if the Michael addition or the strain-promoted cycloaddition techniques were employed. Instead, using the Staudinger–Bertozzi ligation the AuNP-CRGDK bioconjugate could be synthesized efficiently and with a high loading onto the nanomaterial.

Finally the Staudinger-AuNPs can be used also in material chemistry. Thanks to their clean way of reacting they can react easily with any azide modified surface or material for the

creation of nanohybrid materials and sensors. We are currently exploring these possibilities.

Acknowledgements

We (RHEH, MSW) acknowledge the Natural Sciences and Engineering Research Council of Canada and The University of Western Ontario financial support. PG thanks the Government of Canada for a Vanier Scholarship and Research Western.

Notes and references

1 A. Kumar, H. L. Ma, X. Zhang, K. Y. Huang, S. B. Jin, J. Liu, T. Wei, W. P. Cao, G. Z. Zou and X. J. Liang, *Biomaterials*, 2012, **33**, 1180–1189.
2 A. J. Mieszawska, W. J. M. Mulder, Z. A. Fayad and D. P. Cormode, *Mol. Pharmaceutics*, 2013, **10**, 831–847.
3 D. Xi, S. Dong, X. X. Meng, Q. H. Lu, L. J. Meng and J. Ye, *RSC Adv.*, 2012, **2**, 12515–12524.
4 Y. C. Yeh, B. Creran and V. M. Rotello, *Nanoscale*, 2012, **4**, 1871–1880.
5 C. J. Murphy, A. M. Gole, J. W. Stone, P. N. Sisco, A. M. Alkilany, E. C. Goldsmith and S. C. Baxter, *Acc. Chem. Res.*, 2008, **41**, 1721–1730.
6 S. Eustis and M. A. El-Sayed, *Chem. Soc. Rev.*, 2006, **35**, 209–217.
7 D. Pissuwan, T. Niidome and M. B. Cortie, *J. Controlled Release*, 2011, **149**, 65–71.
8 J. B. Delehanty, K. Boeneman, C. E. Bradburne, R. Kelly, J. E. Bongard and I. L. Medintz, *Ther. Delivery*, 2010, **1**, 411–433.
9 W. R. Algar, D. E. Prasuhn, M. H. Stewart, T. L. Jennings, J. B. Blanco-Canosa, P. E. Dawson and I. L. Medintz, *Bioconjugate Chem.*, 2011, **22**, 825–858.
10 N. J. Agard, J. M. Baskin, J. A. Prescher, A. Lo and C. R. Bertozzi, *ACS Chem. Biol.*, 2006, **1**, 644–648.
11 S. S. van Berkel, M. B. van Eldijk and J. C. M. van Hest, *Angew. Chem., Int. Ed.*, 2011, **50**, 8806–8827.
12 P. Gobbo, Z. Mossman, A. Nazemi, A. Niaux, M. C. Biesinger, E. Gillies and M. S. Workentin, *J. Mater. Chem. B*, 2013, **2**, 1764–1769.
13 K. E. Beatty, J. D. Fisk, B. P. Smart, Y. Y. Lu, J. Szychowski, M. J. Hangauer, J. M. Baskin, C. R. Bertozzi and D. A. Tirrell, *ChemBioChem*, 2010, **11**, 2092–2095.
14 P. V. Chang, J. A. Prescher, E. M. Sletten, J. M. Baskin, I. A. Miller, N. J. Agard, A. Lo and C. R. Bertozzi, *Proc. Natl. Acad. Sci. U. S. A.*, 2010, **107**, 1821–1826.
15 M. Chigrinova, C. S. McKay, L. P. B. Beaulieu, K. A. Udachin, A. M. Beauchemin and J. P. Pezacki, *Org. Biomol. Chem.*, 2013, **11**, 3436–3441.
16 X. Wang, P. Gobbo, M. Suchy, M. S. Workentin and R. H. E. Hudson, *RSC Adv.*, 2014, **4**, 43087–43091.
17 E. Saxon and C. R. Bertozzi, *Science*, 2000, **287**, 2007–2010.
18 S. H. Yoshimura, S. Khan, S. Ohno, T. Yokogawa, K. Nishikawa, T. Hosoya, H. Maruyama, Y. Nakayama and K. Takeyasu, *Bioconjugate Chem.*, 2012, **23**, 1488–1493.
19 A. Watzke, M. Kohn, M. Gutierrez-Rodriguez, R. Wacker, H. Schroder, R. Breinbauer, J. Kuhlmann, K. Alexandrov, C. M. Niemeyer, R. S. Goody and H. Waldmann, *Angew. Chem., Int. Ed.*, 2006, **45**, 1408–1412.
20 M. B. Soellner, K. A. Dickson, B. L. Nilsson and R. T. Raines, *J. Am. Chem. Soc.*, 2003, **125**, 11790–11791.
21 D. E. Borchmann, N. T. Brummelhuis and M. Weck, *Macromolecules*, 2013, **46**, 4426–4431.
22 C. I. Schilling, N. Jung, M. Biskup, U. Schepers and S. Brase, *Chem. Soc. Rev.*, 2011, **40**, 4840–4871.
23 M. King and A. Wagner, *Bioconjugate Chem.*, 2014, **25**, 825–839.
24 B. E. Ramakers, J. C. van Hest and D. W. Lowik, *Chem. Soc. Rev.*, 2014, **43**, 2743–2756.
25 D. Grohmann, F. Werner and P. Tinnefeld, *Curr. Opin. Chem. Biol.*, 2013, **17**, 691–698.
26 H. C. Wu, J. Q. Yu and J. B. Spencer, *Org. Lett.*, 2004, **6**, 4675–4678.
27 P. Gobbo and M. S. Workentin, *Langmuir*, 2012, **28**, 12357–12363.
28 K. D. Hartlen, H. Ismaili, J. Zhu and M. S. Workentin, *Langmuir*, 2012, **28**, 864–871.
29 J. Zhu, B. M. Lines, M. D. Ganton, M. A. Kerr and M. S. Workentin, *J. Org. Chem.*, 2008, **73**, 1099–1105.
30 J. He, X. L. Huang, Y. C. Li, Y. J. Liu, T. Babu, M. A. Aronova, S. J. Wang, Z. Y. Lu, X. Y. Chen and Z. H. Nie, *J. Am. Chem. Soc.*, 2013, **135**, 7974–7984.
31 H. Y. Lee, S. H. R. Shin, A. M. Drews, A. M. Chirsan, S. A. Lewis and K. J. M. Bishop, *ACS Nano*, 2014, **8**, 9979–9987.
32 P. Gobbo, S. Novoa, M. C. Biesinger and M. S. Workentin, *Chem. Commun.*, 2013, **49**, 3982–3984.
33 J. C. Azcarate, M. A. F. Addato, A. Rubert, G. Corthey, G. S. K. Moreno, G. Benitez, E. Zelaya, R. C. Salvarezza and M. H. Fonticelli, *Langmuir*, 2014, **30**, 1820–1826.
34 F. L. Lin, H. M. Hoyt, H. van Halbeek, R. G. Bergman and C. R. Bertozzi, *J. Am. Chem. Soc.*, 2005, **127**, 2686–2695.

